VENUSIAN TESSERAE: MORPHOLOGIC VARIATION IN BACKSCATTER COEFFICIENT AND TOPOGRAPHY DATASETS. R. S. Albach[1] and J. L. Whitten[1], [1] Department of Earth and Environmental Sciences, Tulane University, New Orleans, LA (ralbach@tulane.edu).

Introduction: Tesserae are regions of high radar backscatter and tectonic deformation that cover ~8% of the surface of Venus [1]. Despite being the oldest stratigraphic units on Venus [1], many open questions about tesserae remain like their composition(s), surface modification since emplacement, and formation mechanism. Proposed formation mechanisms include upwelling or downwelling of the mantle [2, 3]. Tesserae material has been variously proposed to be basaltic or felsic [4, 5]. To explore these theories, we compare a global morphologic map of tesserae with multiple datasets, including those from Magellan and those of other researchers.

Comprehensive global studies aimed at determining the composition and formation mechanism(s) of tesserae are limited by available global datasets of the surface of Venus from the Magellan mission (SAR, emissivity, topography), VIRTIS on Venus Express, and low-resolution radar data from the Arecibo radio telescope. Previous global mapping efforts do not divide all tesserae by morphology [1, 6], although many regional maps do have comprehensive morphologic divisions of individual tessera [7–12]. Using the results of our -global morphologic mapping of Venusian tesserae, we can see clear differences in the radiophysical properties of some morphologies, as well as the elevation trends. The global morphologic map is also compared with global observations of radar emissivity and topography differences between regions of tesserae [e.g.,13], aside from surface morphology.

Methodology: The Magellan SAR left look global mosaic (spatial resolution of 75 meters per pixel) was used to map tesserae based on morphology at a scale of 1:750,000. Morphologies are defined by the spacing, the shape, and the orientation of the tectonic features such as the graben, fractures, and ridges that compose tesserae. See previous LPSC abstract for details on the defined morphologies and their extents [14]. Each instance of a morphologic texture was mapped as an individual polygon.

To produce a backscatter coefficient raster, a Python code using the Geospatial Data Abstraction Library (GDAL) was used to process the Magellan Left Look Mosaic line by line. The latitude of each line was used to find the appropriate incidence angle of the Magellan SAR with respect to the surface [15, their Table 1A]. The inputs of the backscatter coefficient equation from [15] include the digital number value of each pixel and the correct incidence angle for the latitude of the pixel (Eqn. 1).

$$\sigma_o = 10^{0.1[-20+(DN-1)/5]} \frac{0.0118\cos(\phi+0.5)}{[\sin(\phi+0.5)+0.111\cos(\phi+0.5)]^3}$$

Eqn. 1: Backscatter coefficient equation [15], σ_o = backscatter coefficient, Φ = incidence angle, DN = digital number.

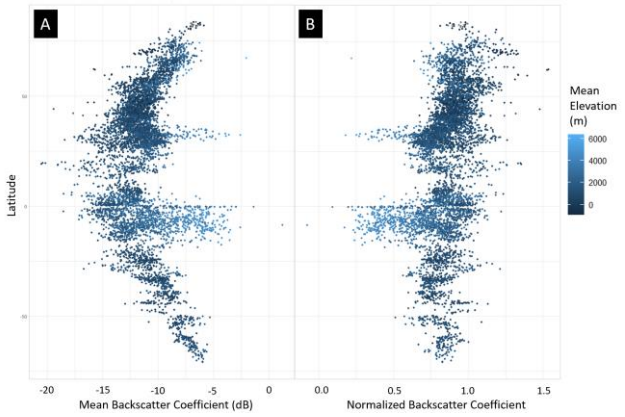

Fig. 1: (A) Mean backscatter coefficient of all mapped polygons plotted against latitude. (B) Normalized mean backscatter coefficient of all mapped polygons plotted against latitude.

The resulting backscatter coefficient raster was used to calculate summary statistics of all mapped polygons. Comparison of the resulting backscatter coefficient dataset showed a remaining strong latitudinal dependance in a parabolic shape (Fig. 1a). With the latitude (also incidence angle) as the overriding signal controlling mean backscatter coefficient patterns, the dataset had to be normalized. Normalization was done using the average DN value of the tesserae, 120, and the corresponding backscatter coefficient was calculated at each latitude and all data points at those latitudes were divided by their corresponding normalizing backscatter coefficient. The resulting dataset no longer retains latitudinal effects (Fig. 1b).

Additionally, two topography datasets were compared to the morphologic map: a spatially limited, higher resolution stereotopography dataset [16] and the 5 km/pixel resolution Magellan topography dataset. Comparison of two different spatial resolution topography datasets allows an assessment of observed elevation trends by tessera morphology and different wavelength topographic patterns in the tesserae.

Preliminary Results: Mapped morphologies included the following: L, sets of graben; R, orthogonal sets of intersecting lineations; SP, parallel and sinuous

ridges; M, intersecting and sinuous ridges; F, finely spaced lineations; VP, block-like features with fine scale lineations and surrounded by topographic lows; AR, hummocky with ridges surrounded by semi-circular topographic lows; D, highly diffuse and parallel ridges; N, bright, squiggly ridges with radar-dark surroundings [14]. The normalized mean backscatter coefficient shows little variation across morphologic categories (Fig. 2). The backscatter coefficient skews higher at high elevations, corresponding to areas of tesserae which may have radar-bright material properties [17, 18].

Polygons were categorized as ferroelectric, semiconductors, or undetermined in composition based on emissivity elevation trends [13]. Comparing the normalized mean backscatter coefficient of textural categories with the compositional classification from [13] shows that composition may influence backscatter coefficient more than texture-related characteristics like roughness. Ferroelectric polygons are predominantly lower in normalized backscatter coefficient across all textures than the semiconductor polygons or the undetermined polygons (Fig. 2). Semiconductor and undetermined tesserae plot closely together and only in texture VP do the semiconductor and ferroelectric mean backscatter coefficient plot closely together.

Topographic datasets show that some textures occur predominantly at lower elevations (e.g., texture F) while others occur at higher elevations (textures AR, D). Similar trends are visible in both the higher resolution [16] and lower resolution topographic datasets.

Discussion and Conclusions: Backscatter coefficient similarity between tessera morphologies globally could indicate several things. 1) The methodology for calculating backscatter coefficient, which was developed relative to the volcanic plains of Venus, is ineffective for differentiating tesserae. 2) There may be an overriding signal in the backscatter coefficient of tesserae because it is a radiophysical property that can convey roughness, material composition, and other geologic constraints. Therefore, composition may be a more important control on backscatter coefficient than the roughness scale of mapped textural variations. For example, the correlation between normalized mean backscatter coefficient and material compositions defined on the basis of emissivity [13] may be indicative of the backscatter coefficient being predominantly controlled by composition. Because some tesserae may, on the whole, have a higher backscatter coefficient than other tesserae, it will be important to compare trends as normalized to each tessera, allowing a fairer comparison across the global population of tesserae.

References: [1] Ivanov M. & Head J. (1996) JGR, 101, 14861-14908. [2] Phillips R. et al. (1991) Science, 252, 651-658. [3] Bindschadler et al. (1992) JGR, 97, 13495-13532. [4] Ivanov M. (2001) Solar System Research, 35, 1-17. [5] Mueller N. et al. (2008) JGR, 113, E00B17. [6] Senske D. A. et al. (1994) LPSC XXV, 1245-1246 (abs.). [7] Gilmore M. & Head J. (2018) Planetary and Space Science, 154, 5–20. [8] Bindschadler D. et al. (1992) JGR, 97, 13563–13577. [9] Hansen V. & Willis J. (1996) Icarus, 123, 296–312. [10] Bindschadler D. & Head J. (1991) JGR, 96, 5889–5907. [11] Bruegge R. & Head J. (1989) GRL, 16, 699-702. [12] Bender K. et al. (2000) Icarus, 148, 153-159. [13] Brossier J. & Gilmore M. (2021) Icarus, 355, 114161. [14] Albach R. & Whitten J. (2020) LPSC LII, 2232 (abs.). [15] Campbell B.A. (1995) USGS Open-File Report 95-519. [16] Herrick R. et al. (2012) Eos, 93, 125-126. [17] Harrington E. & Treiman A.H. (2015) LPSC XLVI, 2713 (abs). [18] Klose K.B. et al. (1992) JGR, 97, 16353-16369.

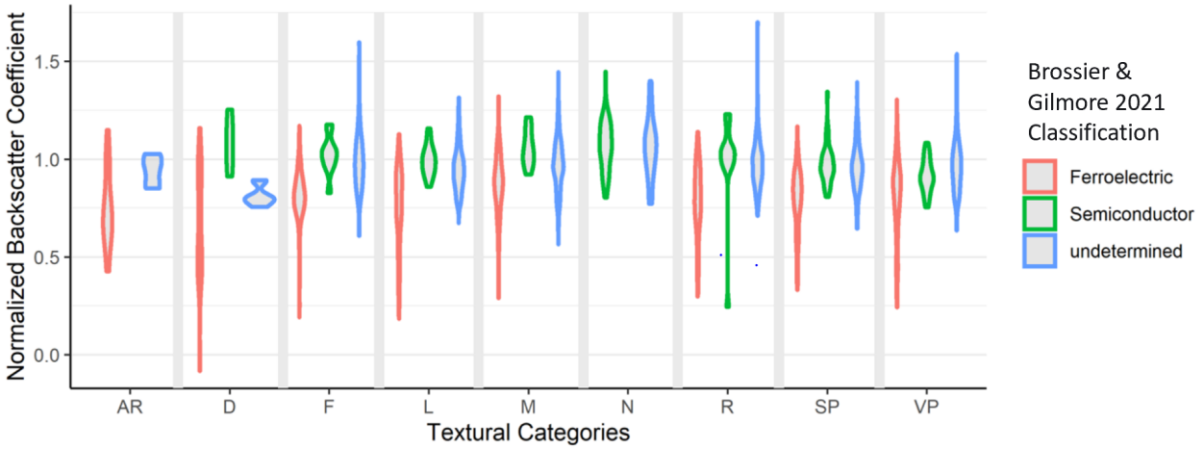

Fig. 2: Mean normalized backscatter coefficient of all polygons in each textural category. Violin plots show the density of the normalized backscatter coefficient for each tessera classification (ferroelectric, semiconductor, and undetermined) from [13].